ACS APPLIED ENERGY MATERIALS

www.acsaem.org Article

Carbonized Bacterial Cellulose-Derived Binder-Free, Flexible, and Free-Standing Cathode Host for High-Performance Stable Potassium−Sulfur Batteries

Apurva Anjan,[§] Vikram Kishore Bharti,[§] Chandra Shekhar Sharma, and Mudrika Khandelwal*

Cite This: *ACS Appl. Energy Mater.* 2023, 6, 3042−3051 Read Online

ACCESS | Metrics & More | Article Recommendations | Supporting Information

ABSTRACT: In search of improved advanced energy storage systems to meet our fast-growing energy demands for large-scale applications, potassium−sulfur batteries (KSBs) provide an essential alternative due to their high specific capacity apart from the low cost and abundance of potassium and sulfur. However, the insulating nature of sulfur, volume changes, and shuttle effect impede the development of these batteries. Further, the binder, carbon additives, and current collector used in the assembly of cells in a conventional approach decrease the energy density of cells. To overcome these challenges, we propose a binder-free and free-standing carbonized bacterial cellulose (CBC) as a cathode host that not only provides a conducting pathway but also has a porous network that is resilient to volume change. To ensure the uniform loading of sulfur, CBC was dipped into the sulfur/carbon disulfide solution, followed by melt diffusion at 160 °C to prepare a sulfur-infused CBC (S-CBC) cathode. This S-CBC cathode with an interconnected fiber network delivers a significantly high reversible capacity of 1311 mA h g^{-1} at a current density of 50 mA g^{-1}. While connected for long-term cycling, the potassium sulfur cell delivers an initial reversible capacity of 475 mA h g^{-1} at 100 mA g^{-1}. Once the cell is stabilized after 80 cycles, it maintains a capacity of 123 mA h g^{-1} with a capacity retention of 86% after 500 cycles. This enhanced electrochemical performance of flexible and free-standing S-CBC cathode is further analyzed using first-principles calculations. Moreover, the efficacy of the S-CBC cathode is also tested under high sulfur loading (1.6 and 2.4 mg cm^{-2}, respectively) for the practical development of KSBs.

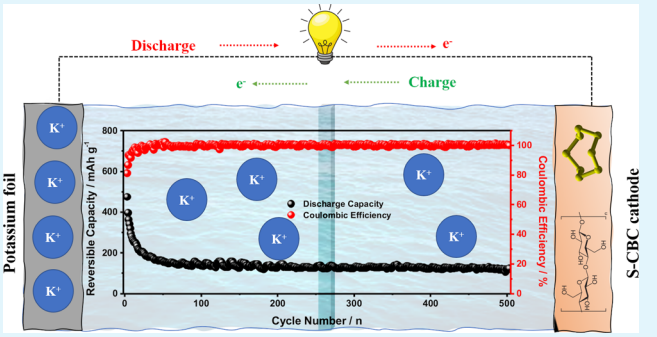

KEYWORDS: *carbonized bacterial cellulose, binder free, free-standing and flexible cathode, first-principles calculation, potassium-sulfur batteries*

1. INTRODUCTION

The global demand for clean energy is ever increasing with large-scale applications in electric vehicles and grid storage. Currently used lithium-ion batteries (LIBs), due to their limited energy density (∼200−220 W h kg^{-1}), cannot meet these requirements.[1−3] Therefore, much attention has been paid to exploring alternative next-generation energy storage technologies over the past decade or so.[4] Meanwhile, the lithium-sulfur battery that uses a lithium anode coupled with a sulfur cathode has emerged as an appealing candidate as it can offer a high energy density of 2567 W h kg^{-1}.[5] However, the limited availability and, therefore, the high cost of lithium hinder their use in large-scale applications.[6,7] On the contrary, potassium, the eighth-most abundant metal in the earth's crust, has the potential to replace lithium as an anodic material.[8] Potassium has a weaker Lewis acidity and offers a low standard reduction potential (−2.93 V vs standard hydrogen electrode), resulting in high ion mobility and conductivity. A sulfur cathode with a very high capacity of 1675 mA h g^{-1}, when coupled with a potassium anode, can deliver a high theoretical gravimetric energy density of 914 W h kg^{-1}.[9,10]

However, in a typical potassium−sulfur battery (KSB), the practical applications are restricted due to several issues. First, the insulating nature of sulfur (5×10^{-15} S cm^{-1}) and potassium disulfide (K_2S) results in the low utilization of active sulfur.[11] Second, the large size of potassium ions leads to a massive volume variation (∼309%) in KSB and results in electrode pulverization and deterioration.[11] Third, the dissolution of intermediate potassium polysulfides develops a concentration gradient and diffuses to the anode, giving rise to

Received: December 27, 2022
Accepted: February 14, 2023
Published: February 22, 2023

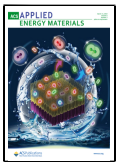

https://doi.org/10.1021/acsaem.2c04157
ACS Appl. Energy Mater. 2023, 6, 3042−3051

Scheme 1. Schematic of the Synthesis Route for the S-CBC Cathode

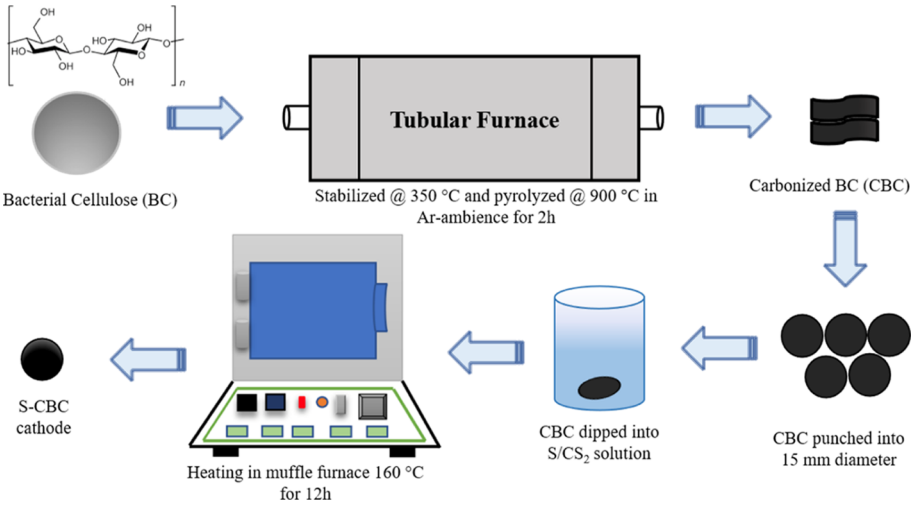

the infamous shuttle effect, which causes anode corrosion, self-discharge, limited cyclability, and low Coulombic efficiency.[12]

To circumvent these issues, several nanostructured carbonaceous materials such as microporous carbon,[13] carbon nanotubes (CNT)s,[14] and so on have been used as a sulfur host to improve the electrochemical performance in KSBs. Zhao et al.[15] synthesized a series of ordered mesoporous carbon/sulfur composites as cathodes with different sulfur amounts using a melt-diffusion process. The composite was further coated with polyaniline to enhance conductivity. The cell could retain a capacity of 329.3 mA h g^{-1} after 50 cycles at 50 mA g^{-1}. Covalently confined sulfur was also used as a modified cathode as another strategy to achieve enhanced and stable performance with a capacity retention of up to 86% (~253 mA h g^{-1} after 300 cycles at 150 mA g^{-1}).[16] In yet another report, iodine-doped sulfurized polyacrylonitrile was used as a cathode delivering ~700 mA h g^{-1} after 100 cycles at the rate of 0.1 C with ~74% capacity retention.[17]

However, these strategies may not serve the purpose of the development of practical KSBs primarily for two reasons: (i) sulfur loading is too low (<0.5 mg/cm^2), and (ii) cell fabrication includes electrochemical inactive species such as binders (for proper adhesion of the electrode slurry to the current collector), additives (to increase the conductivity), and current collectors (for providing a conducting pathway). The use of a binder, carbon additives, and current collector has always been an issue because these components do not participate directly in the electrochemical reaction and thus increase the dead weight of the battery and lead to decreased energy density. In this direction, Yuan et al.[14] used CNT films prepared by floating catalyst vapor deposition to form a self-supported, binder-free cathode matrix. Sulfur (S) was dispersed on CNT films, followed by a melt-diffusion strategy to incorporate sulfur. The as-fabricated cell with S/CNT composite exhibited a capacity of 135 mA h g^{-1} after 200 cycles with a capacity retention of 23.1%. Further, Yuan et al.[18] used activated carbon cloth fiber (ACF) with different specific surface areas as a binder-free matrix and mixed it with sulfur to obtain an ACF@S composite cathode. The as-prepared ACF@S cathode delivered a capacity of 157 mA h g^{-1} after 250 cycles with a capacity retention of 50%.

In this work, for the first time to the best of our knowledge, we present a flexible and free-standing mesoporous bacterial cellulose-derived carbon as a cathode matrix to host sulfur, which can be directly used with potassium foil as the counter electrode without a binder. Bacterial cellulose (BC), a biopolymer cultured using various grades of bacteria, is the purest form of cellulose with a three-dimensional interwoven nanofibrous structure.[19−21] When pyrolyzed in the inert atmosphere, it yields carbonized bacterial cellulose (CBC), an interconnected assembly of CNF that enables the smooth transaction of electrons to carry out the redox reaction with sulfur. Moreover, the porous structure of CBC not only helps to sustain the volume changes during potassiation/depotassiation but also enables higher sulfur loading for practical purposes. For a uniform and higher sulfur loading, sulfur was added to the carbon disulfide (CS_2) solvent. CBC was soaked into this solution before the melt diffusion, unlike the conventional way of sulfur infusion in the solid powder form. The electrochemical testing performed using a flexible and free-standing CBC matrix to host sulfur (S-CBC) as a cathode for KSB further reflects these benefits. The cyclic voltammogram confirms the two-step reduction process of sulfur, resulting in an impressive capacity of 1311 mA h g^{-1} at 50 mA g^{-1}. Moreover, the cell retained 86% capacity even after 500 continuous charge/discharge cycles, reflecting the stable performance of S-CBC.

2. MATERIALS AND METHODS

2.1. Materials. Dextrose, yeast extract, peptone, sodium phosphate, and citric acid anhydrous were obtained from Sisco Research Laboratories Pvt. Ltd., India. Sulfur, potassium cubes, potassium trifluoromethanesulfonimide (KTFSI), and tetra ethylene glycol dimethyl ether (TEGDME) were received from Sigma-Aldrich, India. Carbon disulfide (CS_2) was obtained from Alfa Aesar, India. The glass microfiber filter separator was purchased from GE Healthcare Life Sciences, India. All the chemicals were used as received without further purification.

2.2. Preparation of BC. Bacterial cellulose was cultured using the standard Hestrin and Schramm (HS) media. The HS media was prepared by adding 20 g glucose, 5 g yeast extract, 5 g peptone, 3.4 g sodium phosphate, and 1.14 g citric acid in 1 L of deionized (DI) water.[22] The pH of the media was maintained at 3.5. The prepared media was autoclaved to kill the other microorganisms and avoid contamination. 100 mL of autoclaved media was poured into a 15 mm diameter glass Petri plate, followed by the addition of 3 mL bacterial inoculum (acetobacter xylinum) with uniform dispersion inside a laminar airflow cabinet. The Petri plate was sealed with parafilm to

https://doi.org/10.1021/acsaem.2c04157
ACS Appl. Energy Mater. 2023, 6, 3042−3051

avoid excess oxygen. The sealed Petri plate was transferred to an incubator maintained at 25 °C in static mode. After 14 days, thick white pellicles were collected from the culture plate and washed in 0.5 M NaOH solution. The pellicles were washed thoroughly with DI water for a few days until the pH reached the neutral level (7.0) and were used for further experiments.[22]

2.3. Synthesis of CBC. The formed BC pellicles were freeze-dried for 24 h before the carbonization to remove the associated water. Freeze-dried BC pellicles were cut in rectangular shapes (2.5 × 6 cm) and then transferred to a tubular furnace in a ceramic crucible while maintaining an inert atmosphere using argon gas. The carbonization was carried out in two steps.[23] First, it was stabilized at 350 °C for 2 h with a heating rate of 2 °C min^{-1}, followed by the carbonization at 900 °C for 2 h with a heating rate of 5 °C min^{-1}. After the natural cooling of the furnace, the free-standing CBC was collected and used to impregnate the sulfur, as discussed below.

2.4. Synthesis of Free-Standing S-CBC. CBC was roll-pressed to a sheet-like structure and cut into 15 mm diameter by a punching machine. The circular CBC was dipped into an appropriate amount of S/CS_2 solution for 2 h.[24] It was then taken out of the solution and left in the ambient atmosphere for 2 h for the complete evaporation of CS_2. For thorough infiltration of sulfur in CBC, it was heated in a sealed stainless-steel autoclave at 160 °C for 12 h. The as-prepared S-CBC cathode could be used directly as a cathode in potassium−sulfur batteries. We used different sulfur loadings to prepare S-CBC cathodes: the lower loading was 0.6 mg cm^{-2}, and the higher loading was 1.6 and 2.4 mg cm^{-2}. A detailed schematic for cathode preparation is shown in Scheme 1.

2.5. Material Characterizations. The resulting samples (CBC and S-CBC) were investigated structurally using the X-ray diffraction (XRD) patterns recorded using Rigaku Smart Lab high-resolution XRD with Cu Kα (λ = 0.154 nm) in 2θ ranges of 10° and 70°. Raman spectrum was collected using a Jobin Yvon spectrometer to quantify a graphitic and disordered structure, utilizing an HR 800 micro-Raman laser (excitation wavelength of 594 nm). The morphology of CBC and S-CBC was observed by a focused ion beam scanning electron microscope (JIB-4700F), and elemental mapping was analyzed by energy dispersive spectroscopy (EDAX). To quantify the amount of sulfur in the composite, thermogravimetric analysis (TGA) was performed on SDT Q600 V20.9 from room temperature to 900 °C in a nitrogen atmosphere. Bruker TENSOR 37 was used to record Fourier-transform infrared (FTIR) spectroscopy.

2.6. First-Principles Calculations. Density functional theory was used to perform the first-principles calculations. Gaussian software with B3LYP/6-31G theory level was used to perform the analysis. The total binding energy of the reaction (ΔE_T) was computed as

$$\Delta E_T = \Delta E_{product} - \Delta E_{reactant}$$
$$= \Delta E\ (K_2S_6 \text{ interacted with different structures})$$
$$- [\Delta E\ (\text{pristine structure}) + \Delta E\ (K_2S_6)]$$

where $\Delta E_{product}$ and $\Delta E_{reactant}$ are the total ground state energy of the product and reactant for a given reaction.[25−28] K_2S_6 was chosen as a representing molecule for soluble polysulfides.

2.7. Electrochemical Measurements. The flexible and binder-free S-CBC cathode (active material) was adopted as an electrode. Potassium foil was used as a reference/counter electrode, and Whatman glass microfiber filters were used as a separator. The electrolyte used was 3 M KTFSI in TEGDME. The amount of electrolyte in each cell was 80 μL. The CR2032 coin-type cells were assembled inside the glovebox maintained under an argon ambiance. The cell was galvanostatically charged−discharged (GCD) between 0.8 and 3.0 V vs (K/K^+) at various current densities on Biologic VSP 300. The cyclic voltammetry (CV) measurement was carried out in a potential range of 0.8−3.0 V at a scan rate of 0.1 mV s^{-1}. Electrochemical impedance spectroscopy (EIS) data were obtained with Biologic VSP 300 in a frequency range of 0.01 Hz to 1.0 MHz. All the testing was performed at room temperature.

2.8. Symmetric Cell Measurements. CBC was used as both reference and counter electrode for symmetric cell measurements. 80 μL of 3.0 M KTSFI in TEGDME solvent with and without the addition of 0.5 M K_2S_6 (1:1 by v/v %) was used as the electrolyte. The cell was swept in a voltage window of −1.0 to 1.0 V at a scan rate of 25 mV s^{-1}.

3. RESULTS AND DISCUSSION

3.1. Physiochemical Characterizations. The flexible and free-standing S-CBC electrodes were prepared using an S/CS_2 solution followed by melt diffusion, as discussed in the previous section. The morphology of as-prepared CBC and S-CBC was examined using FIB-SEM and is shown in Figure 1.

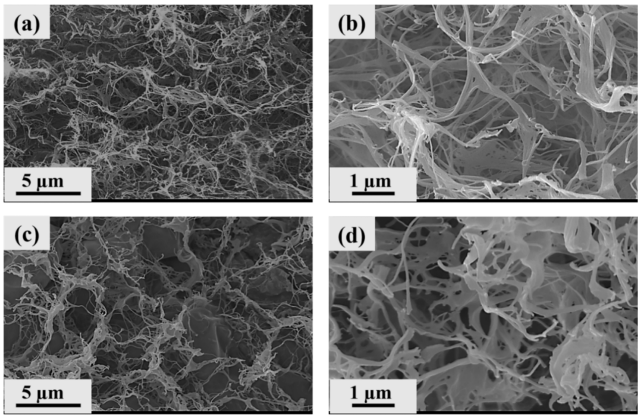

Figure 1. FIB-SEM images of (a,b) CBC and (c,d) S-CBC.

CBC consisted of an interconnected CNF and porous structure (specific surface area: 541.3 m^2 g^{-1}, pore volume: 3.93 cm^3 g^{-1}),[29] as shown in Figure 1a,b. The fibrous networks were stacked layer by layer to form a three-dimensional continuous architecture. This interconnected network provided a continuous linkage between the nanofibers, which is beneficial for enhanced electron transport. S-CBC also showed the CNF morphology with an interconnected network (Figure 1c,d). Even after melt diffusion, no sulfur aggregation could be seen, proving its uniform distribution into the CBC. The remaining volume void in the S-CBC provides free space and helps accommodate the massive volume expansion during potassiation and depotassiation. To confirm the elemental composition and distribution, EDAX was performed and is shown in Figures S1, S2. CBC revealed the presence of carbon and oxygen (Figure S1), whereas S-CBC revealed the presence of sulfur, carbon, and oxygen (Figure S2). Sulfur was evenly distributed throughout the matrix, which is a potential benefit for the efficient and high utilization of sulfur owing to conductive pathways imparted by CNFs.

The XRD investigated the nature of carbon in CBC and sulfur infused in S-CBC. The XRD patterns of CBC and S-CBC are shown in Figure 2a. CBC showed a broad peak at ∼ 24° corresponding to the (002) plane and ascribed to the presence of amorphous carbon.[30] However, after composite preparation, the crystalline peaks of sulfur dominated over the amorphous carbon. The diffraction patterns of S-CBC matched precisely with the orthorhombic phase of sulfur (JCPDS: 08-0247).[31] Further, the diffraction pattern of the sulfur powder was carried out to investigate any reduction occurring after the composite preparation. The figure shows that the diffraction patterns of sulfur and S-CBC match well; thus, it can be

https://doi.org/10.1021/acsaem.2c04157
ACS Appl. Energy Mater. 2023, 6, 3042−3051

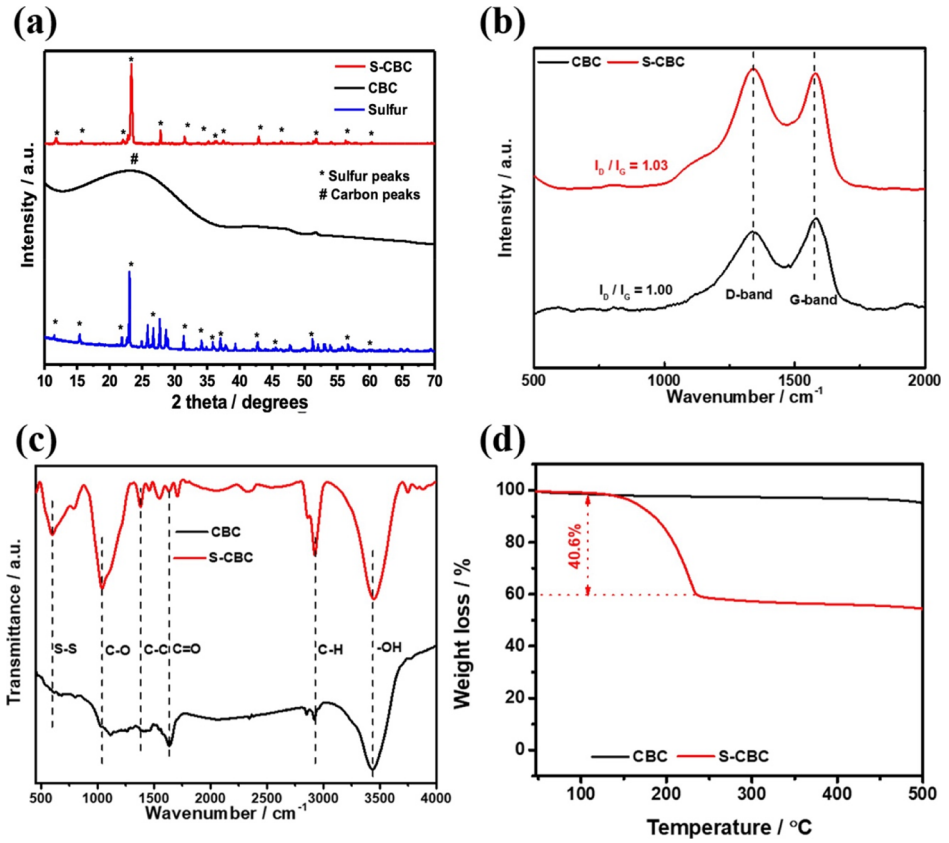

Figure 2. Physico-chemical characterizations: (a) XRD patterns, (b) Raman spectra, (c) FTIR spectra, and (d) TGA of CBC and S-CBC at a heating rate of 10 °C min^{-1} in N_2 atmosphere.

concluded that there is no phase change for sulfur after composite preparation. Raman spectroscopy was carried out to further analyze the carbon structure as XRD revealed the dominance of sulfur, and thus, the carbon structure was not observed in S-CBC (Figure 2b). Raman spectra of CBC and S-CBC showed two different peaks positioned at 1343 and 1584 cm^{-1}. The peak at 1343 cm^{-1} can be ascribed to the D-band, which stands for the sp^3 hybridized carbon (unsaturated dangling bond) and non-continuous graphitic (disordered) structure. However, the peak at 1584 cm^{-1} can be ascribed to the G-band, which stands for sp^2 hybridized carbon (saturated bond) and long-range graphitic structure.[32] To quantify the degree of graphitization,[33] the I_D/I_G ratio was calculated to observe the dominance of graphitic or disordered structures. The I_D/I_G ratio values were 1.00 and 1.03 for CBC and S-CBC, respectively. It further reflects that the sulfur infusion is not distorting the carbon structure.

The presence of a functional group in the cathode matrix determines the interaction of polysulfides during the redox reaction. FTIR analysis was performed to study the functional groups in both CBC and S-CBC (Figure 2c). CBC revealed the presence of −OH, C−H, C═O, C−C, and C−O functional groups attached to the carbon skeleton.[30] However, after composite preparation, S-CBC revealed an additional peak of ∼595 cm^{-1}, which stands for S−S bridging.[16] This observation also supports the successful sulfur infusion in the carbon skeleton. Identification of these functional groups is further used to calculate the interaction of soluble polysulfide (K_2S_6) to understand which functional group is more beneficial for capturing soluble polysulfides. Additionally, capacity values need to be evaluated based on sulfur infusion. Therefore, the evaluation of sulfur content is a crucial step. For that, TGA was performed in N_2 atmosphere at a heating rate of 10 °C min^{-1}, illustrated in Figure 2d. The TGA profile of CBC showed some weight loss beyond 250 °C, which can be associated with the loss of the −OH functional group as revealed by FTIR spectroscopy. Meanwhile, S-CBC showed a very stable configuration up to 130 °C, which can be related to composite heating at 160 °C (where the loss of the −OH group already occurred). S-CBC showed a very steep loss after 155 °C, which can be related to the loss of sulfur, and based on weight loss in this regime, sulfur content was calculated as 40.6% by weight.

3.2. First-Principles Calculations. The presence of an oxygen functional group may enhance the dipole moment (due to the high electronegativity of the oxygen atom) and thus help trap the soluble polysulfides. Therefore, first-principles calculations were performed based on the functional group's analysis as per FTIR spectroscopy. The study compares the enhancement in the interaction energy concerning the functional groups. Graphene (Gr) is chosen as a control structure, and functional groups are added to the graphene structure. The optimized structures of graphene (Gr), graphene with −OH (Gr_ OH), graphene with C−O (Gr_ C−O), graphene with C═O (Gr_ C═O), and K_2S_6 (as a representing molecule for soluble polysulfides) are shown in Figure 3a−e. The corresponding optimized energy of each structure is shown in Figure S3. Figure 3f represents the interaction energy calculation of Gr_ C═O with K_2S_6. After interaction with Gr_ C═O, K_2S_6 showed distortion in its structure that can be understood as an effect of strong interaction. Therefore, the interaction energy with different functionalities has been plotted in Figure 3g to understand

https://doi.org/10.1021/acsaem.2c04157
ACS Appl. Energy Mater. 2023, 6, 3042−3051

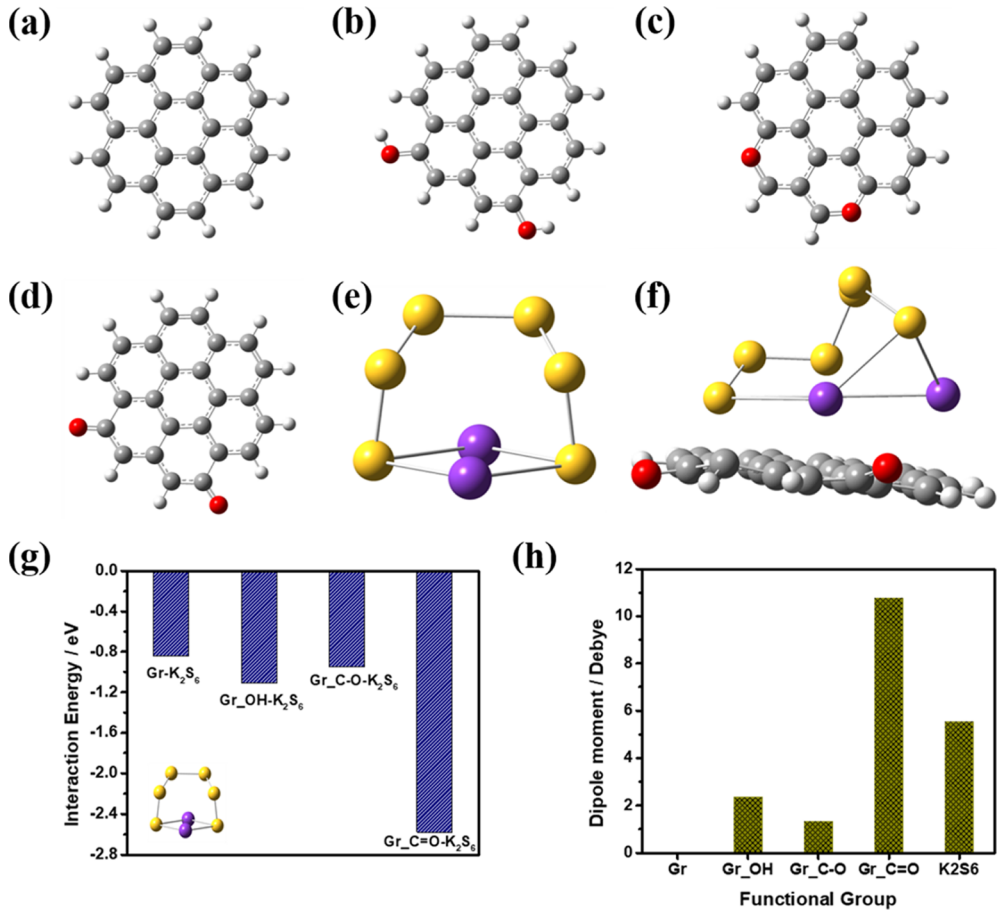

Figure 3. Optimized structure of (a) graphene (Gr), (b) graphene with −OH (Gr_ OH), (c) graphene with C−O (Gr_ CO), (d) graphene with C═O (Gr_ C═O), (e) K_2S_6, and (f) optimized interaction of Gr_ C═O with K_2S_6 (g) interaction energy of the different functional groups with K_2S_6 and (h) variation of dipole moment with different functional groups Gr < Gr_ C−O < Gr_ OH < Gr_ C═O < K_2S_6.

which functional group is more helpful for trapping soluble polysulfides. Figure 3g reveals the following order of interaction energy: Gr−K_2S_6 < Gr_ C−O−K_2S_6, Gr_ OH−K_2S_6 < Gr_ C═O−K_2S_6. Further, the dipole moment is calculated to see the change in polarity with the attached functional group (due to the presence of an electronegative element), as shown in Figure 3h. The dipole moment follows the increasing order of Gr < Gr_ C−O < Gr_ OH < K_2S_6 < Gr_ C═O. The dipole moment of K_2S_6 is higher than that of Gr, Gr_ C−O, and Gr_ OH optimized structures, reflecting that it is a polar molecule, and a polar functional group is beneficial for the interaction to minimize the shuttling behavior of soluble polysulfides. Moreover, the dipole moment also varies in the same order, reflecting that Gr_ C═O has the highest dipole moment. This correlates with the condition that the higher the dipole moment, the stronger the interaction. Therefore, the presence of −C═O is more helpful in trapping polysulfides than the other functional groups in the carbon structure.

3.3. Electrochemical Characterizations. Detailed electrochemical measurements were performed to understand and quantify the redox behavior, charge−discharge capability, and cyclic stability of the as-prepared free-standing S-CBC cathode. First, CV was carried out in the potential window of 0.8−3.0 V at a sweep rate of 0.1 mV s^{-1} and is illustrated in Figure 4a. CV curves reveal the thermodynamic aspect of the electrochemical reaction, and therefore, the reaction pathway can be traced. The CV curve of S-CBC showed a two-step sulfur reduction during the cathodic scan. These two peaks stand for the reduction of elemental sulfur (S_8) to long-chain potassium polysulfides (K_2S_n, $4 \le n \le 8$) and consecutive reduction of K_2S_n to short-chain potassium polysulfides (K_2S_m, $3 \le m \le 1$). Further, the two oxidation peaks are observed during the anodic scan. These two peaks represent the oxidation of K_2S_m back to K_2S_n, followed by oxidation to elemental sulfur (S_8).[16] The presence of two peaks during the cathodic and anodic scans reveals the reversibility of the redox reaction occurring in the cell. The consecutive five cycles of CV curves almost overlapped, indicating excellent reversibility of S-CBC. Moreover, a small peak located at 2.7 V can be ascribed to the formation of the surface−bound complex, thiosulfate ($S_2O_3^{2-}$).[8] The formation of this surface−bound complex can be ascribed to the available functional groups (carbonyl and hydroxyl) in the CBC matrix. Therefore, the interaction of the polysulfides is higher in the presence of a functional group compared to the bare carbon structure (discussed in first-principles calculations).

While the CV demonstrates the thermodynamic behavior, GCD quantifies the kinetic behavior of the material. Therefore, GCD of S-CBC (with a sulfur loading of 0.6 mg cm^{-2}) was performed at 50 mA g^{-1} and is shown in Figure 4b. Assembled KSBs deliver higher capacity in the sloping region, unlike LSBs, whose capacity comes from the constant voltage region. The GCD profile of S-CBC revealed similar attributes in various

https://doi.org/10.1021/acsaem.2c04157
ACS Appl. Energy Mater. 2023, 6, 3042−3051

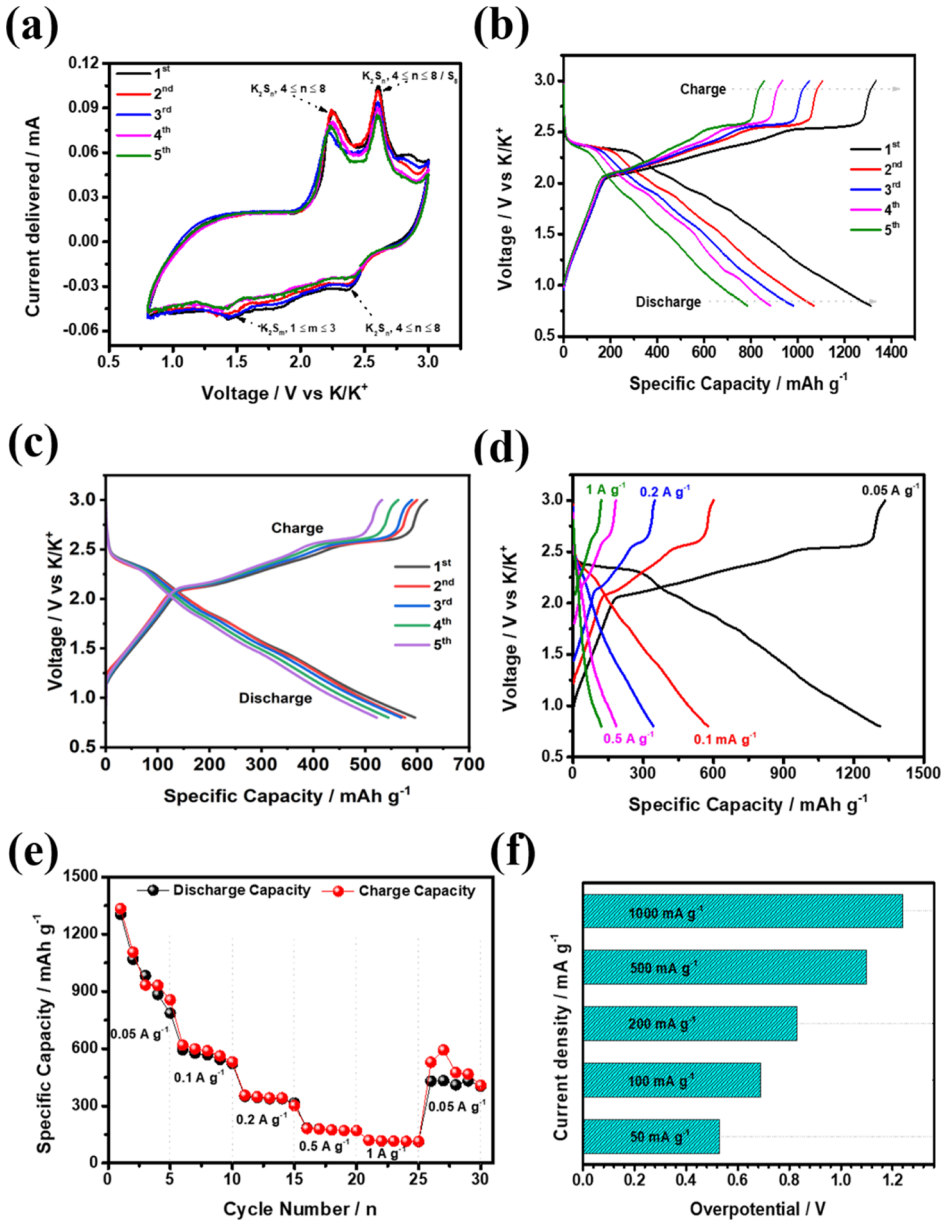

Figure 4. Electrochemical characterizations of S-CBC with areal loading of 0.6 mg cm^{-2}: (a) CV at 0.1 mV s^{-1}; GCD profiles at (b) 50 mA g^{-1}, (c) 100 mA g^{-1}, and (d) different current densities; (e) rate-capability test; (f) overpotential at different current densities.

reports.[14,18] The initial capacity of 1311 mA h g^{-1} was achieved; however, a capacity of 785 mA h g^{-1} was delivered after five cycles. This behavior can be related to the fact that in the KSB system, initially, there will be structural transformation, and thus, capacity degradation can be observed. Later, the GCD was performed at 100 mA g^{-1}, as seen in Figure 4c, to assess the stability of the structure. In the consecutive five cycles at 100 mA g^{-1}, fewer capacity fluctuations were observed, suggesting a stable structure's evolution. An initial capacity of 617 mA h g^{-1} was obtained, which was reduced to 562 mA h g^{-1} after five cycles of GCD at 100 mA g^{-1}.

The rate-capability plot illustrating the capacity values at different current densities is shown in Figure 4d,e. The rate-capability graph indicates that the capacity fluctuations were maximum at 50 mA g^{-1}; however, these were reduced with increasing current density. A stable capacity value was obtained at 100, 200, 500, and 1000 mA g^{-1}, respectively. S-CBC delivered a discharge capacity of 343, 184, and 113 mA h g^{-1} at 200, 500, and 1000 mA g^{-1}, respectively. After cycling at higher current rates, the cell was connected again to 50 mA g^{-1}. Interestingly, the cell did not show the fluctuation observed at the initial stage and delivered a capacity of 595 mA h g^{-1}, which shows the excellent reversibility of the S-CBC cathode once the initial structural evolution was completed.

Overpotential is an evaluation of the polarization of the electrode under a constant current charge−discharge. The overpotential of S-CBC was calculated at various current densities ranging from 50 to 1000 mA g^{-1}, as shown in Figure 4f. The overpotential value at 50, 100, 200, 500, and 1000 mA g^{-1} was 530, 690, 830, 1100, and 1024 mV, respectively. The overpotential showed an increment with the current density. It can be ascribed to the fact that an increase in current density increases polarization.

To assess the electrochemical performance of a higher sulfur-loading electrode (areal loading: 1.6 mg cm^{-2}) for

https://doi.org/10.1021/acsaem.2c04157
ACS Appl. Energy Mater. 2023, 6, 3042−3051

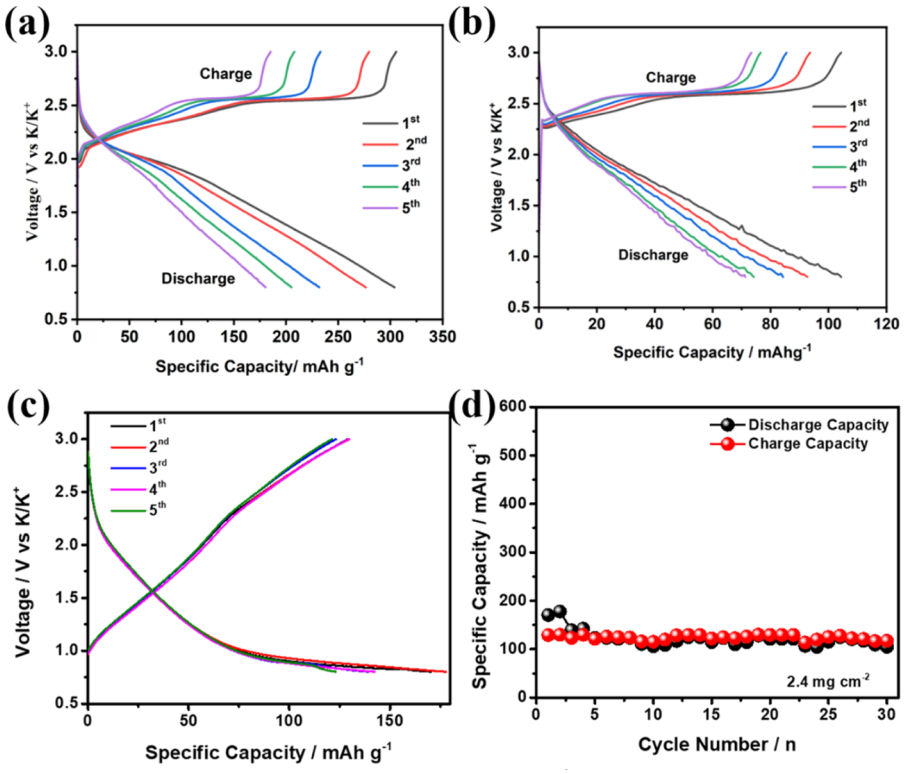

Figure 5. Electrochemical performance with 1.6 mg cm^{-2} electrodes: (a) GCD at 50 mA g^{-1}, (b) GCD at 100 mA g^{-1}; electrochemical performance with 2.4 mg cm^{-2} electrodes: (c) GCD at 50 mA g^{-1}, (d) cyclic stability at 50 mA g^{-1}.

practical application, the GCD profiles were performed at different current densities. The GCD profile obtained at 50 and 100 mA g^{-1} are shown in Figure 5a,b. A similar observation was repeated even with a high sulfur loading electrode. The GCD profiles obtained at 50 mA g^{-1} showed capacity degradation due to structural transformation and thus decreased from 320 to 180 mA h g^{-1} after five cycles. When the current was increased to 100 mA h g^{-1}, the initial capacity was 115 mA h g^{-1} and remained 74 mA h g^{-1} after five consecutive cycles. The decrement in the capacity at 100 mA g^{-1} is much lower than that at 50 mA g^{-1} due to the stabilized structure of the cathode. This observation is in complete agreement with the observation of GCD profiles obtained with low sulfur loading (0.6 mg cm^{-2}) electrodes.

Further, the GCD was carried out with 2.4 mg cm^{-2} electrodes to continue evaluating the material's behavior under high sulfur loading. The GCD profile obtained for the initial five cycles is shown in Figure 5c. The profile nature showed little change, which can be attributed to the feature with a higher loading electrode. The cell delivered an initial discharge capacity of 129 mA h g^{-1} with a coulombic efficiency of 75.6%, which improved with further cycling and reached 100% after five cycles. The cyclic stability was continued for 30 cycles to observe the capacity decay trend under high sulfur loading (Figure 5d). The charge−discharge capacity values were retained for 30 continuous cycles. The capacity retention was calculated based on the initial and final capacity obtained and was 91%. This analysis reveals the efficacy of the S-CBC to be cycled even at higher sulfur loading and thus makes it a suitable candidate for the practical development of KSBs.

Furthermore, the interfacial properties were evaluated for the S-CBC electrode using the EIS method, as shown in Figure 6a. The study was done before and after 100 cycles in a frequency range of 0.01 Hz to 1 MHz. In both these cases, a semicircular region can be seen in the medium- to high-frequency regime and nearly a straight line in the low-frequency region. The semicircular region corresponds to charge transfer resistance (R_{ct}), which indicates the redox reaction taking place where the active material gets an electron from the electrode and potassium ions from the electrolyte. On the other hand, the straight line in the low-frequency region corresponds to potassium ion diffusion resistance (R_w). S-CBC offered a resistance value of 37.7 and 1357 Ω corresponding to R_s and R_{ct}, respectively. However, after cycling, the values increased to 49.6 and 2472 Ω corresponding to R_s and R_{ct}. S-CBC showed an enhancement in the R_s and R_{ct} after cycling. It can be correlated to the deposition of the end discharge product (K_2S) on the S-CBC electrode. K_2S is insulating in nature and thus increases the R_{ct} for S-CBC after cycling. However, the cell operated even for continuous 500 cycles (as shown in long-term cycling) primarily due to its ability to accommodate more K_2S in a porous matrix.

The first-principles calculation reveals the strong interaction of K_2S_6 with CBC. Therefore, to get a better insight into the interaction between CBC and K_2S_6, symmetric CV was performed in a potential range of −1.0 to 1.0 V at a scan rate of 25 mV s^1 (Figure 6b). The CV profile shows that when K_2S_6 was absent in the electrolyte, the current response recorded was null. This indicates that the counter electrode in the symmetric cell cannot contribute to the current. However, when K_2S_6 was added to the electrolyte, the symmetric cell showed a higher current response of 200 μA and an enhanced area under the curve. It reflects that the surface reaction with CBC occurs only in the presence of K_2S_6. This attributes to the CBC cathode's efficient adsorption and interaction of long-chain potassium polysulfides.

https://doi.org/10.1021/acsaem.2c04157
ACS Appl. Energy Mater. 2023, 6, 3042−3051

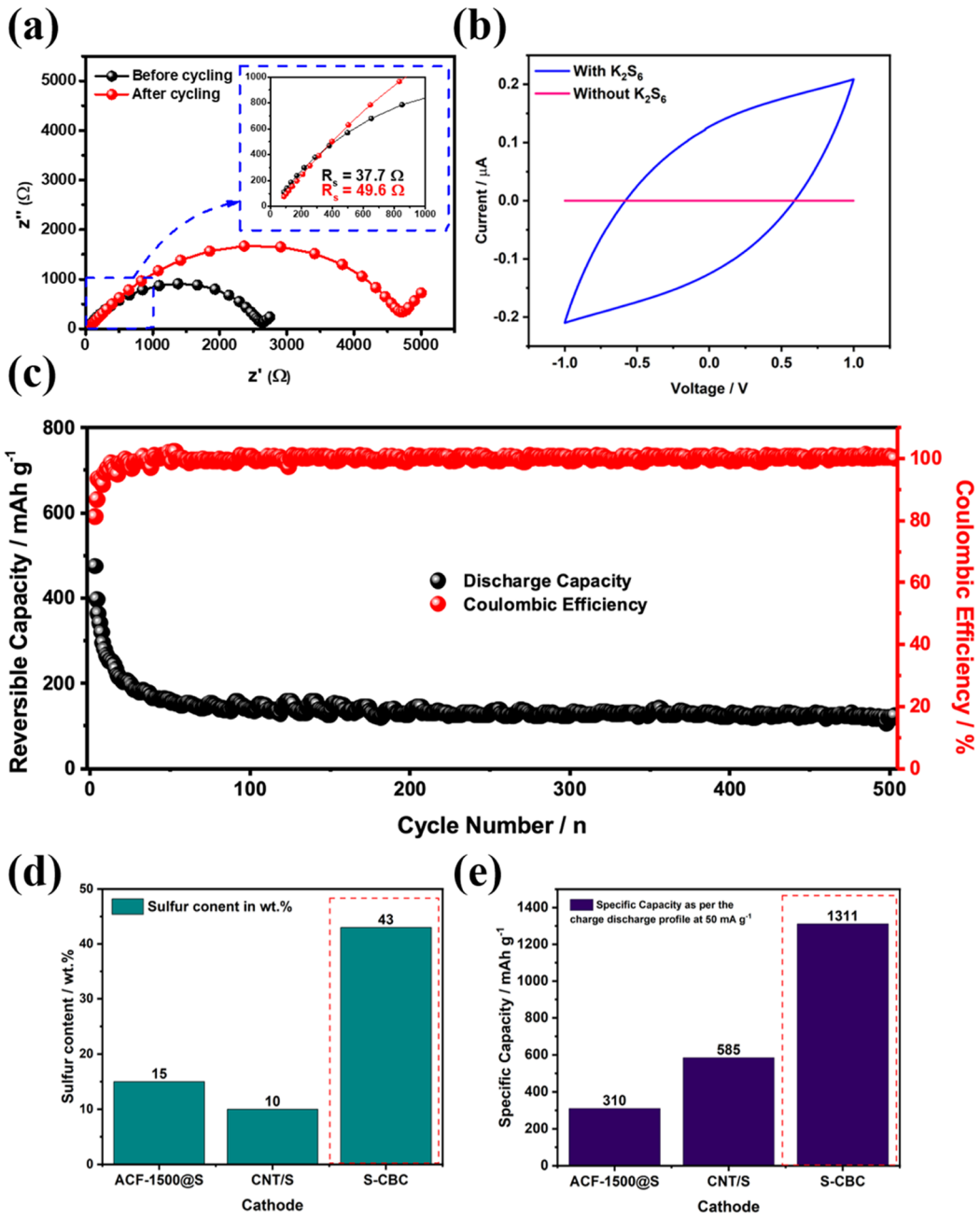

Figure 6. (a) Nyquist plot for S-CBC cathode (before and after cycling); (b) CV curves of symmetric cells at 25 mV s^{-1}; (c) long-term cycling at 100 mA g^{-1}, comparison with the literature; (d) sulfur content; and (e) initial capacity at 50 mA g^{-1}.

In addition, we also evaluated the cycle life of the fabricated cell. Therefore, the long-term cyclic stability of the S-CBC cathode was performed with a fresh cell at a current density of 100 mA g^{-1}. The charge−discharge profiles of the selected cycles are shown in Figure S4. During the first cycle, a high capacity of 475 mA h g^{-1} was obtained; however, the capacity was reduced after 50 cycles. It can be related to the structural transformation occurring in the cathode, as discussed previously. This transformation was observed for initial 80 cycles. Once the structural transformation was established, the cell with S-CBC cathode showed a stable capacity up to 500 cycles. At the end of the 500th cycle, the cell delivered a capacity of 143 mA h g^{-1}. The capacity retention was calculated after the stabilization and was found to be 86%. The long-term stability profile is shown in Figure 6c.

To clearly spell out the superior electrochemical performance of the present work, the results are compared with the existing literature based on the free-standing matrix as presented in Figure 6d,e and Table S1. The comparison is made for the cycle life, capacity retention, areal loading, and capacity to fairly evaluate the performance of S-CBC over the available literature. A careful observation suggests that despite the high sulfur content in the cathode, which is an essential consideration for the practical development of KSBs, we can achieve a higher initial capacity in the present work compared to the literature. Once the structure transformation occurred in the initial cycles, much higher capacity retention, up to 86%,

https://doi.org/10.1021/acsaem.2c04157
ACS Appl. Energy Mater. 2023, 6, 3042−3051

was achieved. As CBC comprises an interconnected network of CNF, it helps in reducing the pathway for electron transactions. The porous morphology of CBC also enables buffering of the volume changes during potassiation and depotassiation. Moreover, the high electrolyte uptake enables the uniform electrolyte−electrode interface; thus, the active sulfur can be utilized more efficiently. These attributes can be considered to be critical reasons for S-CBC's enhanced electrochemical properties over recently reported works in the literature.

To substantiate the effect of volume change upon potassiation and depotassiation, the cycled electrode was examined through FIB-SEM (Figure 7a,b). It may be observed

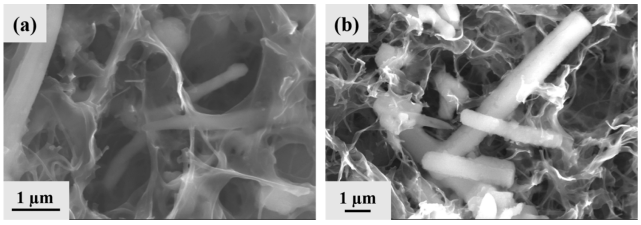

Figure 7. FIB-SEM image of post-cycled S-CBC electrode at (a) 20,000× and (b) 10,000× magnification, respectively.

that the interconnected nanofibrous network remains intact after cycling in the case of S-CBC, and deposition is seen on the fibrous network. This deposited product can be ascribed to the formation of the end-discharge product, K_2S. It can be noted that surfaces and spaces are still available to accommodate discharge products in S-CBC produced during further use (Figure 7b).

4. CONCLUSIONS

In summary, we demonstrated a facile way to prepare a BC-derived CNF-based free-standing, flexible cathode that can directly be used without any binder, additives, or current collector. The sulfur infusion was carried out using an S/CS_2 solution followed by a melt-diffusion to ensure a uniform and higher loading. The potassium sulfur cell with the as-fabricated (S-CBC) cathode delivered an initial reversible capacity of 1311 mA h g^{-1} at a current density of 50 mA g^{-1}. Cyclic stability was performed at 100 mA g^{-1} and showed a capacity of 475 mA h g^{-1} with a capacity retention of 86% after 500 cycles. The electrochemical performance was also investigated with a high sulfur loading cathode (1.6 and 2.4 mg cm^{-2}) to evaluate the potential of the S-CBC cathode for the practical development of KSBs. Further, the first-principles calculation improved our understanding of this enhanced electrochemical performance by investigating the polysulfide's interactions with the cathode host matrix. This study clearly reveals the potential of mesoporous CNF derived from a natural and sustainable precursor, bacterial cellulose, for fabricating the cathode host in realizing the stable and high performance of futuristic potassium sulfur batteries.

■ ASSOCIATED CONTENT

Supporting Information

The Supporting Information is available free of charge at https://pubs.acs.org/doi/10.1021/acsaem.2c04157.

Elemental mapping of CBC and S-CBC, optimized energy of different structures, charge−discharge profile as cycling, and comparative table (PDF)

■ AUTHOR INFORMATION

Corresponding Author

Mudrika Khandelwal − *Cellulose & Composites Laboratory, Department of Materials Science and Metallurgical Engineering, Indian Institute of Technology, Sangareddy 502285 Telangana, India*; Email: mudrika@msme.iith.ac.in

Authors

Apurva Anjan − *Creative & Advanced Research Based on Nanomaterials (CARBON) Laboratory, Department of Chemical Engineering and Cellulose & Composites Laboratory, Department of Materials Science and Metallurgical Engineering, Indian Institute of Technology, Sangareddy 502285 Telangana, India*

Vikram Kishore Bharti − *Creative & Advanced Research Based on Nanomaterials (CARBON) Laboratory, Department of Chemical Engineering and Cellulose & Composites Laboratory, Department of Materials Science and Metallurgical Engineering, Indian Institute of Technology, Sangareddy 502285 Telangana, India*; orcid.org/0000-0002-9909-8217

Chandra Shekhar Sharma − *Creative & Advanced Research Based on Nanomaterials (CARBON) Laboratory, Department of Chemical Engineering, Indian Institute of Technology, Sangareddy 502285 Telangana, India*; orcid.org/0000-0003-3821-1471

Complete contact information is available at: https://pubs.acs.org/10.1021/acsaem.2c04157

Author Contributions

§A.A.and V.K.B contributed equally.

Notes

The authors declare no competing financial interest.

■ ACKNOWLEDGMENTS

The authors acknowledge the partial support from SERB (CRG/2018/004441) to carry out this work. V.K.B. acknowledges the Ministry of Education (MoE) India for financial support under the PMRF scheme. The authors also acknowledge Tulika Vashist for her input in the grammar correction in the original draft. A.A. and V.K.B. acknowledge Sukesh Kumar for performing the SEM analysis. The authors also acknowledge DST-FIST SEM (JEOL JSM 7800F) facility at Materials Science and Metallurgical Engineering (MSME), IIT Hyderabad.

■ REFERENCES

(1) Lin, Z.; Liu, Z.; Dudney, N. J.; Liang, C. Lithium Superionic Sulfide Cathode for All-Solid Lithium−Sulfur Batteries. *ACS Nano* **2013**, *7*, 2829−2833.

(2) Li, N.; Weng, Z.; Wang, Y.; Li, F.; Cheng, H.-M.; Zhou, H. An Aqueous Dissolved Polysulfide Cathode for Lithium−Sulfur Batteries. *Energy Environ. Sci.* **2014**, *7*, 3307−3312.

(3) Huang, Y. The Discovery of Cathode Materials for Lithium-Ion Batteries from the View of Interdisciplinarity. *Interdiscip. Mater.* **2022**, *1*, 323−329.

(4) Wang, M.; Chen, X.; Yao, H.; Lin, G.; Lee, J.; Chen, Y.; Chen, Q. Research Progress in Lithium-Excess Disordered Rock-Salt Oxides Cathode. *Energy Environ. Mater.* **2022**, *5*, 1139−1154.

(5) Ji, X.; Nazar, L. F. Advances in Li−S Batteries. *J. Mater. Chem.* **2010**, *20*, 9821−9826.

(6) Masias, A.; Marcicki, J.; Paxton, W. A. Opportunities and Challenges of Lithium Ion Batteries in Automotive Applications. *ACS Energy Lett.* **2021**, *6*, 621−630 American Chemical Society February.

(7) Li, X.; Chen, W.; Qian, Q.; Huang, H.; Chen, Y.; Wang, Z.; Chen, Q.; Yang, J.; Li, J.; Mai, Y.-W. Electrospinning-Based Strategies for Battery Materials. *Adv. Energy Mater.* **2021**, *11*, 2000845.
(8) Wu, X.; Leonard, D. P.; Ji, X. Emerging Non-Aqueous Potassium-Ion Batteries: Challenges and Opportunities. *Chem. Mater.* **2017**, *29*, 5031−5042.
(9) Chung, S.-H.; Manthiram, A. Current Status and Future Prospects of Metal−Sulfur Batteries. *Adv. Mater.* **2019**, *31*, 1901125.
(10) Medenbach, L.; Adelhelm, P. Cell Concepts of Metal−Sulfur Batteries (Metal = Li, Na, K, Mg): Strategies for Using Sulfur in Energy Storage Applications. *Topics in Current Chemistry*; Springer International Publishing, 2017.
(11) Zhao, X.; Lu, Y.; Qian, Z.; Wang, R.; Guo, Z. Potassium-sulfur Batteries: Status and Perspectives. *EcoMat* **2020**, *2*, No. e12038.
(12) Seh, Z. W.; Sun, Y.; Zhang, Q.; Cui, Y. Designing High-Energy Lithium−Sulfur Batteries. *Chem. Soc. Rev.* **2016**, *45*, 5605−5634.
(13) Xiong, P.; Han, X.; Zhao, X.; Bai, P.; Liu, Y.; Sun, J.; Xu, Y. Room-Temperature Potassium−Sulfur Batteries Enabled by Microporous Carbon Stabilized Small-Molecule Sulfur Cathodes. *ACS Nano* **2019**, *13*, 2536−2543.
(14) Yuan, X.; Zhu, B.; Feng, J.; Wang, C.; Cai, X.; Qin, R. High-Performance Stable Potassium−Sulfur Batteries Enabled by Free-Standing CNT Film-Based Composite Cathodes. *J. Electron. Mater.* **2021**, *50*, 3037−3042.
(15) Zhao, Q.; Hu, Y.; Zhang, K.; Chen, J. Potassium-Sulfur Batteries: A New Member of Room-Temperature Rechargeable Metal-Sulfur Batteries. *Inorg. Chem.* **2014**, *53*, 9000−9005.
(16) Ma, R.; Fan, L.; Wang, J.; Lu, B. Confined and Covalent Sulfur for Stable Room Temperature Potassium-Sulfur Battery. *Electrochim. Acta* **2019**, *293*, 191−198.
(17) Ma, S.; Zuo, P.; Zhang, H.; Yu, Z.; Cui, C.; He, M.; Yin, G. Iodine-Doped Sulfurized Polyacrylonitrile with Enhanced Electrochemical Performance for Room-Temperature Sodium/Potassium Sulfur Batteries. *Chem. Commun.* **2019**, *55*, 5267−5270.
(18) Yuan, X.; Zhu, B.; Feng, J.; Wang, C.; Cai, X.; Qin, R. Free-Standing, Flexible and Stable Potassium−Sulfur Battery Enabled by Controllable Porous Carbon Cloth. *J. Power Sources* **2020**, *480*, 228874.
(19) Iguchi, M.; Yamanaka, S.; Budhiono, A. Bacterial Cellulose—a Masterpiece of Nature's Arts. *J. Mater. Sci.* **2000**, *35*, 261−270.
(20) Huang, Y.; Zhu, C.; Yang, J.; Nie, Y.; Chen, C.; Sun, D. Recent Advances in Bacterial Cellulose. *Cellulose* **2014**, *21*, 1−30.
(21) Scrosati, B.; Garche, J. Lithium Batteries: Status, Prospects and Future. *J. Power Sources* **2010**, *195*, 2419−2430.
(22) Khandelwal, M.; Windle, A. H.; Hessler, N. In Situ Tunability of Bacteria Produced Cellulose by Additives in the Culture Media. *J. Mater. Sci.* **2016**, *51*, 4839−4844.
(23) Demirbaş, A. Relationships between Carbonization Temperature and Pyrolysis Products from Biomass. *Energy Explor. Exploit.* **2004**, *22*, 411−419.
(24) Huang, Y.; Zheng, M.; Lin, Z.; Zhao, B.; Zhang, S.; Yang, J.; Zhu, C.; Zhang, H.; Sun, D.; Shi, Y. Flexible Cathodes and Multifunctional Interlayers Based on Carbonized Bacterial Cellulose for High-Performance Lithium-Sulfur Batteries. *J. Mater. Chem. A* **2015**, *3*, 10910−10918.
(25) Hehre, W.-J.; Ditchfield, R.; Pople, J.-A. SelfConsistent Molecular Orbital Methods. XII. Further Extensions of GaussianType Basis Sets for Use in Molecular Orbital Studies of Organic Molecules. *J. Chem. Phys.* **1972**, *56*, 2257−2261.
(26) Dill, J. D.; Pople, J. A. Self-consistent Molecular Orbital Methods. XV. Extended Gaussian-type Basis Sets for Lithium, Beryllium, and Boron. *J. Chem. Phys.* **1975**, *62*, 2921−2923.
(27) Francl, M. M.; Pietro, W. J.; Hehre, W. J.; Binkley, J. S.; Gordon, M. S.; DeFrees, D. J.; Pople, J. A. Self-consistent Molecular Orbital Methods. XXIII. A Polarization-type Basis Set for Second-row Elements. *J. Chem. Phys.* **1982**, *77*, 3654−3665.
(28) Stephens, P. J.; Devlin, F. J.; Chabalowski, C. F.; Frisch, M. J. Ab Initio Calculation of Vibrational Absorption and Circular Dichroism Spectra Using Density Functional Force Fields. *J. Phys. Chem.* **1994**, *98*, 11623−11627.
(29) Bharti, V. K.; Pathak, A. D.; Sharma, C. S.; Khandelwal, M. Flexible and Free-Standing Bacterial Cellulose Derived Cathode Host and Separator for Lithium-Sulfur Batteries. *Carbohydr. Polym.* **2022**, *293*, 119731.
(30) Illa, M. P.; Sharma, C. S.; Khandelwal, M. Tuning the Physiochemical Properties of Bacterial Cellulose: Effect of Drying Conditions. *J. Mater. Sci.* **2019**, *54*, 12024−12035.
(31) Hu, Y.; Chen, W.; Lei, T.; Jiao, Y.; Wang, H.; Wang, X.; Rao, G.; Wang, X.; Chen, B.; Xiong, J. Graphene Quantum Dots as the Nucleation Sites and Interfacial Regulator to Suppress Lithium Dendrites for High-Loading Lithium-Sulfur Battery. *Nano Energy* **2020**, *68*, 104373.
(32) Mamidi, S.; Gangadharan, A.; Sharma, C. S. Graphite Coated Pyrolyzed Filter Paper as a Low-Cost Binder-Free and Freestanding Anode for Practical Lithium-Ion Battery Application. *Electrochim. Acta* **2019**, *310*, 222−229.
(33) Bharti, V.; Gangadharan, A.; Rao, T. N.; Sharma, C. S. Carbon Soot over Layered Sulfur Impregnated Coconut Husk Derived Carbon: An Efficient Polysulfide Suppressor for Lithium Sulfur Battery. *Mater. Today Commun.* **2020**, *22*, 100717.

https://doi.org/10.1021/acsaem.2c04157
ACS Appl. Energy Mater. 2023, 6, 3042−3051